ACS APPLIED MATERIALS & INTERFACES

www.acsami.org

Research Article

Whispering Gallery Mode Lasing from Perovskite Polygonal Microcavities via Femtosecond Laser Direct Writing

Xiaoyu Tian, Lin Wang, Wei Li, Qianqian Lin,* and Qiang Cao*

Cite This: *ACS Appl. Mater. Interfaces* 2021, 13, 16952−16958

Read Online

ACCESS | Metrics & More | Article Recommendations | Supporting Information

ABSTRACT: Organic−inorganic halide perovskites have excellent intrinsic properties, such as long carrier lifetime, high photoluminescence quantum yield, and high gain, in whispering gallery mode (WGM) cavities by facile vapor self-assembly or solution process, which make them competitive for high-performance microlasers. However, the performance of perovskite-based microlasers is severely limited by the fabrication of microcavities, which results in poor reproducibility and uncontrolled morphology. Herein, we explore a reproducible method which combined thermal co-evaporation with femtosecond (fs) laser direct writing for formamidinium lead iodide ($FAPbI_3$) perovskite polygon-shaped WGM microcavities. The microlasers pumped with the fs laser had a low threshold of 4.0−12.3 $\mu J/cm^2$ and narrow full width at half-maximum of 0.62−1.05 nm. Moreover, size- and shape-dependent WGM lasing performances are also investigated systematically. The results prove that $FAPbI_3$ polygonal microcavities can serve as promising WGM lasers and have great potential for practical optoelectronic applications.

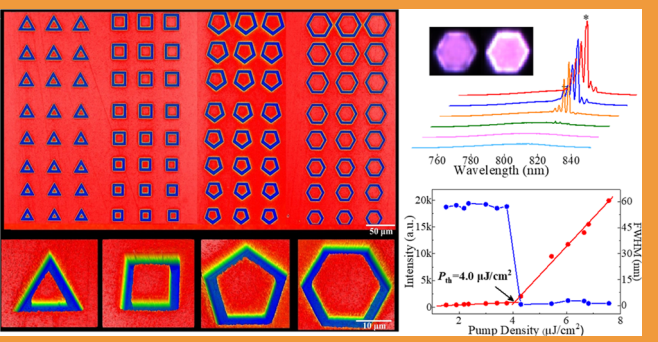

KEYWORDS: *perovskite, femtosecond laser direct writing, polygonal microcavities, whispering gallery mode, near-infrared microlasers*

INTRODUCTION

Xing et al. first found amplified spontaneous emission in perovskite thin films in 2014;[1] since then, the laser behaviors of perovskite have been studied all over the world.[2,3] Lasing had been observed from perovskite cavities with different resonator modes, including whispering gallery mode (WGM) cavity, Fabry−Pérot cavity,[4,5] photonic crystal,[6,7] random cavity,[8,9] plasmon cavity,[10,11] distributed feedback resonator,[12,13] and so on.[14] Among all these cavities, WGM cavities were found to exhibit the strongest confinement effect due to their total internal reflection around the cavities, which results in the excellent optical feedback.[15] Although microsphere, microdisk, and microring WGM microcavities have extremely high Q factors, the isotropic emission along the cavity rim makes it difficult for circular microlasers to efficiently collect the output light.[16,17] It is a straightforward strategy to break the rotational circular symmetry for realizing the directional output emission, through changing the geometrical shape. Regular polygonal microresonator-based microlasers, such as triangular,[18] square,[19] pentagonal,[20] and hexagonal microcavities,[21,22] have been demonstrated to have superior mode properties to those of their circular counterparts.[23]

However, the further development of perovskite polygonal microlasers is severely hindered by the lack of approaches to the scale fabrication of the WGM lasing with low threshold and small volume. So far, many efforts have been made to fabricate large-scale polygonal microresonators. For example, the vapor phase deposition method has been utilized by Li et al.[24] to prepare PbI_2 triangular nanoplates, which exhibit a high Q factor ~2600 at room temperature. Zhang et al.[25] employed the vapor phase epitaxy method to prepare $CsPbX_3$ (X = Cl, Br, and I) single crystal for fabricating high-quality WGM microcavities, reaching a low threshold of about 2 $\mu J/cm^2$. Nevertheless, both the shape and the size of the as-fabricated perovskite microcavities are uncontrollable, which makes it difficult to reveal the underlying connection between the shape and the lasing performance of the polygonal perovskite microcavities.

In this work, we demonstrated a simple, flexible scalable solution that can precisely fabricate and control the morphology of the perovskite polygonal microcavities, by using a femtosecond (fs) laser to directly write the microcavities on the pre-deposited $FAPbI_3$ perovskite films. The thermal co-evaporation method is used for deposing the $FAPbI_3$ perovskite films. Patterned microresonators with different geometry, including triangle, square, pentagonal, and hexagonal microcavities were successfully fabricated by

Received: December 13, 2020
Accepted: March 23, 2021
Published: April 1, 2021

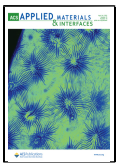

accurately controlling the writing path of the fs laser. The as-fabricated polygonal microcavities match WGM well. Moreover, the size- and shape-dependent WGM lasing performances are also investigated systematically. The hexagonal $FAPbI_3$ microcavity was demonstrated to exhibit the lowest pump threshold (~4.0 $\mu J/cm^2$) and the narrowest full width at half-maximum (fwhm) (~0.62 nm) among all polygonal microcavities. The realized high-quality perovskite polygonal microcavities, with a low pump threshold and narrow fwhm, have a broad application prospect in the field of optoelectronic integration.

RESULTS AND DISCUSSION

Since Liu et al. demonstrated that the thermal co-evaporation method can be used to get highly uniform $MAPbI_3$ films and achieve a photovoltaic efficiencies (PCEs) of ~15.4% of perovskite solar cells,[26] it has gained a lot of attention for use in other perovskite devices.[27−29] An advantage of the thermal co-evaporation method is that it is not so sensitive to the substrate defects (such as dust particles or pinholes) and the problems of uneven solvent evaporation. In this work, we first prepare $FAPbI_3$ films on quartz substrates by the thermal co-evaporation strategy (Figure 1a). Figure 1b shows the crystal

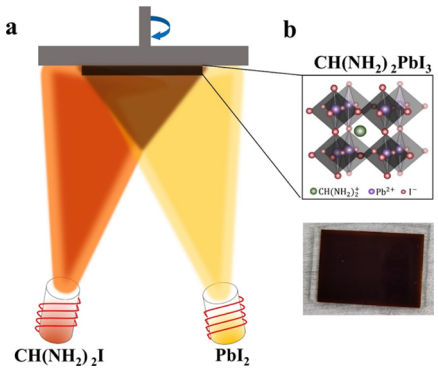

Figure 1. $FAPbI_3$ perovskite films. (a) Schematic diagram of thermal co-evaporation. (b) Crystal structure and photograph of $FAPbI_3$ perovskite films.

structure of $FAPbI_3$ and photograph of $FAPbI_3$ thin films prepared. The as-prepared $FAPbI_3$ thin film is very dense and smooth. As seen in Figure S1 (Supporting Information), we tested atomic force microscopy of the spin-coated and evaporated perovskite films for comparison. This result shows that evaporated films have lower surface roughness (R_q ~ 10.5 nm) and smaller grain size than spin-coated films. Besides, through X-ray diffraction (XRD) patterns (Figure S2, Supporting Information), it can be observed that there are two strong diffraction peaks at approximately 14 and 28°, corresponding to the (110) and (220) planes of the black α-phase perovskite,[30] which indicate the absence of impurities in the as-prepared $FAPbI_3$ thin films. Photoluminescence (PL) and absorption spectrum of the $FAPbI_3$ film are shown in Figure S3 (Supporting Information). The $FAPbI_3$ film shows a strong PL peak at ~790 nm under 532 nm continuous laser excitation and has a strong absorbance of about 790 nm from the ultraviolet to near-infrared region, which is the same as the previous research studies, indicating that $FAPbI_3$ has potent light harvesting capabilities.[31]

The $FAPbI_3$ polygonal microcavities with different configurations are then fabricated by employing the fs laser direct writing on $FAPbI_3$ films along specific paths to depict the triangular, square, pentagonal, and hexagonal microcavities, as shown in Figure 2. The side length of the polygons ranges from 10 to 17 μm (Figure 2a), according to the magnified cross-sectional profile image (Figure 2b) of 10 μm microcavities. We observed no visible damage in the microcavity boundaries and highly smooth surface with low surface roughness. The corresponding height profiles of individual $FAPbI_3$ microcavity with heights of ~124 nm are shown in Figure S5 (Supporting Information). With high crystallinity of $FAPbI_3$ films, highly smooth surface, and ideal perfect polygonal shape, the $FAPbI_3$ microcavities are very suitable for high-quality WGM resonators with outstanding optical performance. A highly repetitive process of the fs laser to write directly is a good way to study the internal mechanism of perovskite microcavity laser and provide the possibility for the diversity of perovskite microlasers.

The perimeters of all $FAPbI_3$ polygonal microcavities are very close, with an edge length (L) of ~26, 19, 15, and 13 μm for the triangular, square, pentagonal, and hexagonal microcavities, respectively. The 532 nm fs laser was utilized to investigate the lasing performances of the as-fabricated microcavities, as seen in Figure S6 (Supporting Information). Using the method which set the sharp blade on a microstage and moved it precisely, we recorded the power of the blade of different positions and calibrated that the spot size of the pump laser beam is ~46 μm, as seen in Figure S7 (Supporting Information). During the experiment, we slightly adjusted the height of 50× microscope objective to ensure pump laser complete coverage to polygonal microcavity, the image of laser spot recorded with charge-coupled device (CCD), as shown in Figure S7 inset (Supporting Information). As shown in Figure 3a,d,h,k, for all $FAPbI_3$ polygonal microcavities, as the pump density increases, a series of periodic peaks will appear, indicating the occurrence of multimode lasing action. In principle, both WGM and F−P mode could happen for polygonal microcavities. We have performed the optical PL images above the lasing threshold of a typical polygonal microcavity (thickness ~124 nm; edge lengths ~26, 19, 15, and 13 μm), as shown in Figure 3a,d,h,k inset. When pump density is higher than the threshold, lasing can be coupled to polygonal microcavity edges, indicating a dominated WGM confinement. In WGM microcavity, efficient optical gain is achieved by total internal reflection around the polygonal microcavities. We plotted fwhm and laser peak intensity (marked with *) versus pump density, respectively, as shown in Figure 3b,e,i,l. The thresholds of lasing for all $FAPbI_3$ polygonal microcavities are estimated to be ~12.3 $\mu J/cm^2$ (triangular), 7.1 $\mu J/cm^2$ (square), 4.8 $\mu J/cm^2$ (pentagonal), and 4.0 $\mu J/cm^2$ (hexagonal), respectively.

The magnified spectra of the lasing mode for all polygonal microcavities are exhibited in Figure 3c,f,g,m, which can be well-fitted by using the Lorentz function. The linewidths of the lasing peaks are as narrow as ~1.05 (triangular), 0.96 (square), 0.78 (pentagonal), and 0.62 nm (hexagonal), respectively, which are comparable to those reported.[18,32,33] The outstanding lasing performance benefits a lot from enough smooth surfaces and edges of $FAPbI_3$ polygonal microcavities, which provide high reflectivity "mirrors" to minimize the dissipation from surfaces. Moreover, we find that both the lasing threshold and the peak linewidth are decreased with the increase of the edge numbers of the cavities. Among all polygonal microcavities, the hexagonal microcavity exhibits the lowest lasing

https://doi.org/10.1021/acsami.0c21824
ACS Appl. Mater. Interfaces 2021, 13, 16952−16958

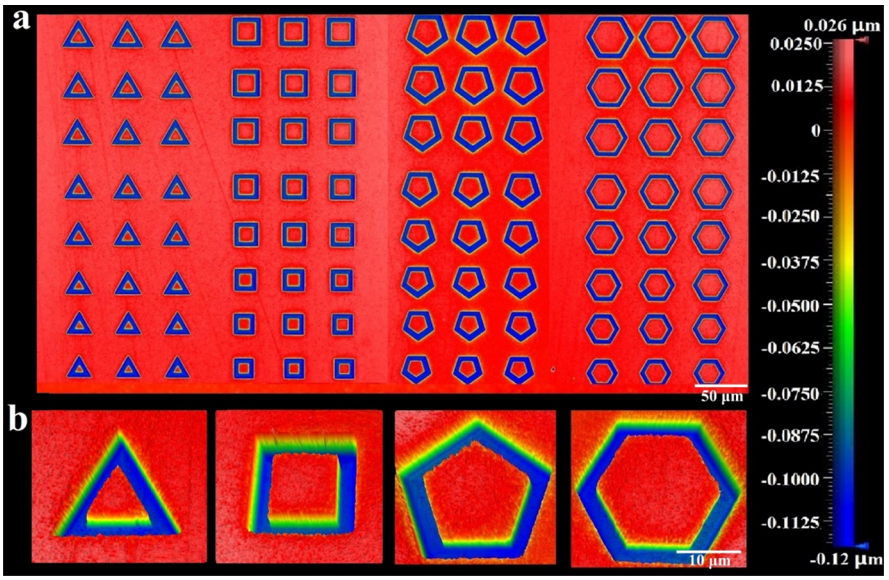

Figure 2. Patterned $FAPbI_3$ microcavities, including triangular, square, pentagonal, and hexagonal. (a) Three-dimensional images of microcavity arrays with edge length from 10 to17 μm. (b) Magnified side profile of perovskite polygon microcavities with an edge length of 10 μm.

threshold (~4 $\mu J/cm^2$) and the narrowest peak linewidth with a value of ~0.62 nm.

In order to stabilize the oscillation in a cavity and strengthen the light, the coherent phase changing round the cavity should satisfy the resonance conditions that is an integer multiple of 2π, that is,[34]

$$nL' = m\lambda \tag{1}$$

where n represents the phase refractive index of the crystal, L' represents round-trip distance, and m denotes the order of the mode. According to the resonance conditions, only the light of a specific frequency can be finally enhanced in the microcavity. Mode spacing $\Delta\lambda$ between the adjacent laser mode is provided to analyze laser features, which is given by the following equation

$$\Delta\lambda = \frac{\lambda^2}{n_g L'} \tag{2}$$

where n_g is the group refractive index and can be expressed as follows

$$n_g = n\left(1 - \frac{\lambda dn}{n d\lambda}\right) \tag{3}$$

The WGM is located around the cavity, which is closely related to the perimeter. For example, $L' = 3\sqrt{3}L$ is used as an approximate value of hexagonal microcavity.

To further explore the wave localization, we vary the edge length (L) of the hexagonal $FAPbI_3$ microcavity from ~9 to ~18 μm and investigate the corresponding laser performance. Figure 4a exhibits the lasing modes from hexagonal cavities with different edge lengths. We find that the mode spacing ($\Delta\lambda$) is linearly decreased with increasing the edge length (L), as exhibited in Figure 4b. The laser spectra with different pump intensities for the other polygonal $FAPbI_3$ microcavities with different edge lengths are also investigated, which present the linear relationship between $\Delta\lambda$ and $1/L$ (Figures S8–S11, Supporting Information). These results demonstrate that all $FAPbI_3$ polygonal microcavities are well matched to the WGM. Besides, from these linear relationships (Figures S8j, S9l, S10l and 4b), the group refractive indices (ng) (~3.35, ~2.62, ~2.77, and ~3.56) obtained at 810 nm.

The evolution of the laser threshold in $FAPbI_3$ polygonal microcavities is also studied. Interestingly, we find that the laser threshold decreases and then increases with increasing the perimeter for all polygonal microcavities, as seen in Figure 4c. For WGM resonator with small size (<76 μm), during increasing the size of cavity, the overlap between the optical mode path confined in cavity and the gain medium decreases, which results in the optical mode "spills" out of the microcavity along the boundary. This is due to the fact that the confinement ability (Γ) is proportional to the lateral size, and the increase of the lasing threshold can be related to the decreasing microcavity size.[35] This result proves that we can realize single-mode lasing in small-size microcavities with the expense of the lasing threshold, and there will be no lasing when the perimeter increases to a certain value, owing to which cavity losses are bigger than the optical gain. However, large-size microcavities (L > 76 μm) need more consideration. The charge carrier trapping at surface states will influence more for coherent light emission performance. The surface volume has an inverse relationship with the crystallite size, and the surface charge carrier trapping effect has an inverse relationship with the cavity size.[36] The $FAPbI_3$ films in this work are prepared by the thermal co-evaporation approach. The grain size of $FAPbI_3$ by thermal evaporation is much smaller than the edge length (L) (Figure S4, Supporting Information). Therefore, the trapping states are mainly located on the surface and uniformly distributed in the film, that is why we get the different behaviors in terms of the edge length-dependent threshold. In a previous work, we have studied the relationship between the diameter of the perovskite microdisk and the laser threshold and got a consistent result.[37] This means that the conclusion is reliable.

Besides, we also find that the fwhm of the lasing peak and the pump threshold are decreasing with increasing the polygonal microcavity order. For the m-faceted polygonal WGM microcavity, the Q factor can be expressed as[38]

https://doi.org/10.1021/acsami.0c21824
ACS Appl. Mater. Interfaces 2021, 13, 16952−16958

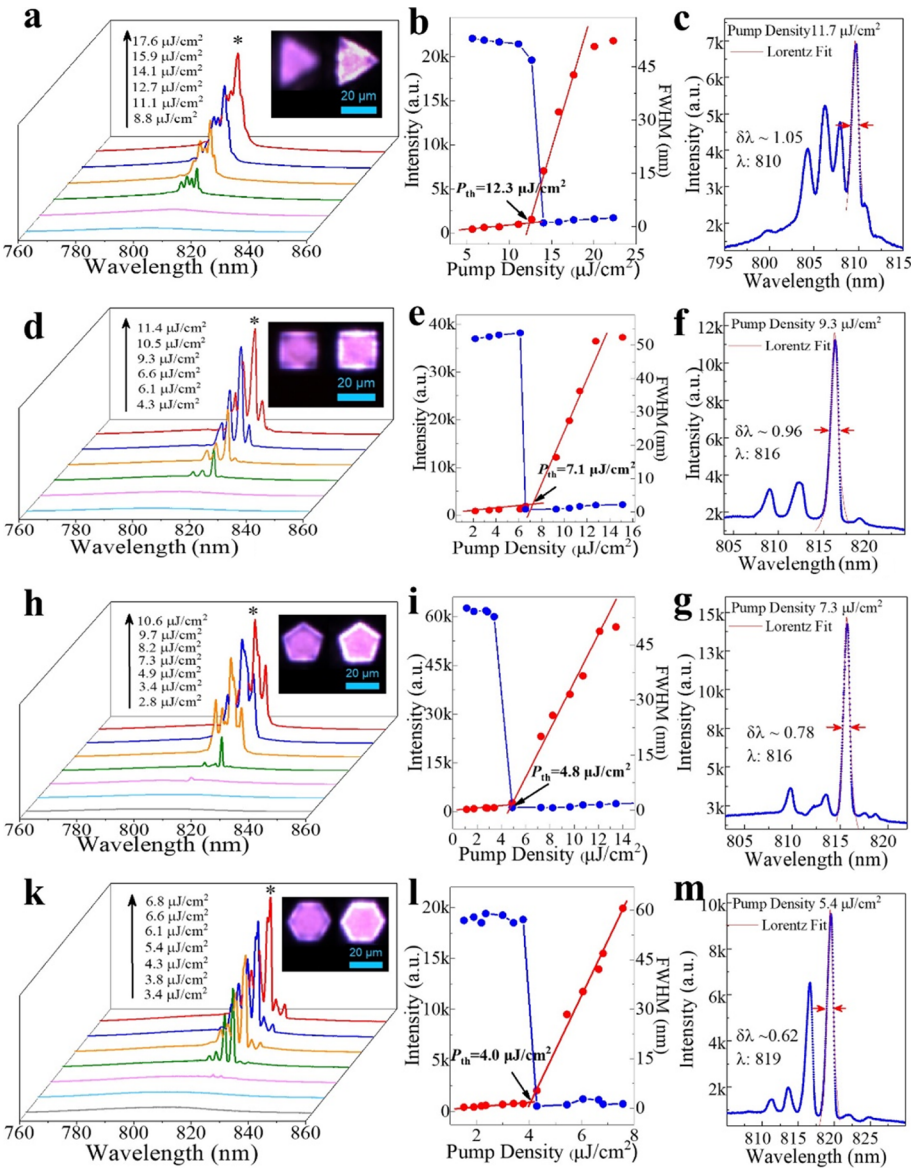

Figure 3. Lasing characterization of $FAPbI_3$ polygonal microcavities (triangular, square, pentagonal, and hexagonal). (a,d,h,k) Emission spectra of a typical $FAPbI_3$ polygonal microcavity at different optical pump density ranging from 8.8 to 17.6, 4.3 to 11.4, 2.8 to 10.6, and 3.4 to 6.8 $\mu J/cm^2$, respectively, displaying the transition process from spontaneous emission to lasing emission. Inset: fluorescence image of an individual polygon microcavity below P_{th} and above P_{th}. The thickness of the polygonal microcavities is the same (about 124 nm), and the edge lengths are 26, 19, 15, and 13 μm, respectively. (b,e,i,l) Intensity as a function of pump density, indicating thresholds of ~12.3, 7.1, 4.8, and 4.0 $\mu J/cm^2$. (c,f,g,m) Magnified emission spectrum above the threshold. The fwhm ($\delta\lambda$) are ~1.05, 0.96, 0.78, and 0.62 nm.

$$Q = \frac{\pi D m n R^{m/4}}{2\lambda(1 - R^{m/2})} \sin\frac{2\pi}{m} \quad (4)$$

where D is the diameter of the polygon circumcircle and m and R are the number and the reflectivity of polygonal cavity facets, respectively. Taking into account the cavity loss at the corner, the light will not converge at the corner of the WGM microcavity, so the total internal reflectance is reasonable.[39,40] This can well explain why the peak linewidth decreases with the microcavity polygonal order. The behavior that lasing threshold decreases with the microcavity polygonal order for approximately same perimeters is consistent with above-mentioned results that P_{th} is inversely proportional to the $\beta \times Q$ product, where the larger Q factor and β (spontaneous emission coupling factor) could indicate a lower threshold.[41,42] The hexagonal microcavity has better light confinement ability compared with other polygonal microcavities because it can eliminate the scattering of edges and corners more.

In order to realize the practical application of perovskite-based optoelectronic devices for lasers in the future, the longevity lifetime is the important problem which needs to be solved. A square $FAPbI_3$ microcavity with L = 19 μm was excited by 532 nm fs pulsed laser (pulse width: 267 fs; repetition rate: 5 kHz) continuous illumination above P_{th} at room temperature (about 23.8 °C, 41% relative humidity). The lasing emission intensity (marked with *) remained stable for 60 min under continuous illumination (Figure 5a). Compared with $CH_3NH_3PbI_3$ ($MAPbI_3$) square microcavity with L = 19 μm, the $FAPbI_3$ exhibited better photostability. The lasing emission intensity (marked with *) from $MAPbI_3$ square microcavity starts to decrease in ~10 min continuous illumination (Figure 5b), and the time-dependent lasing

https://doi.org/10.1021/acsami.0c21824
ACS Appl. Mater. Interfaces 2021, 13, 16952−16958

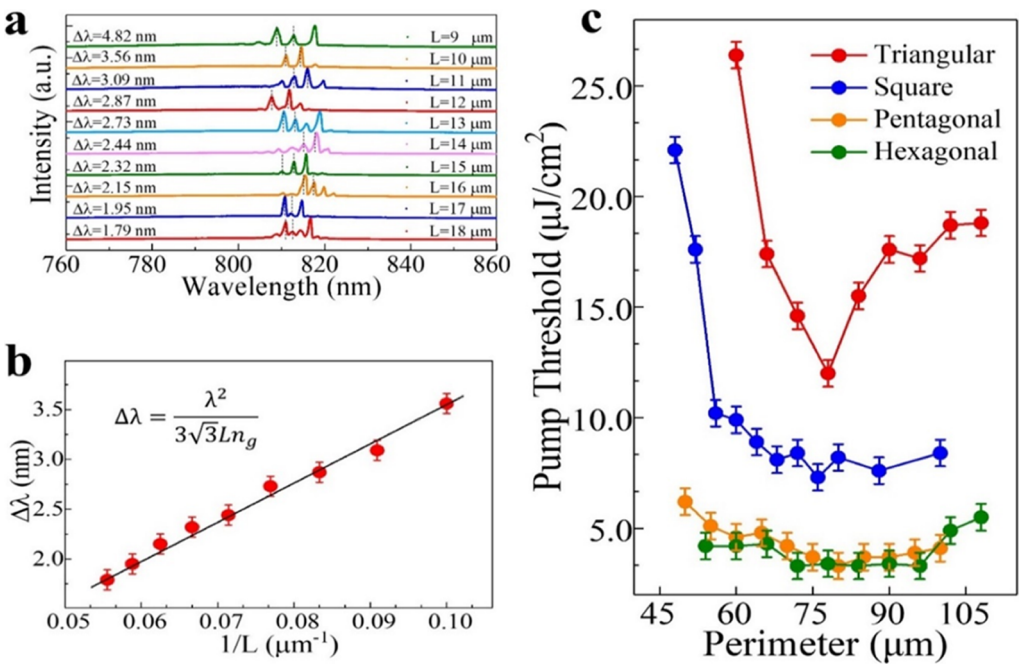

Figure 4. WGM characterization of $FAPbI_3$ hexagonal cavities and the relationship between the lasing threshold and perimeter of $FAPbI_3$ polygon cavities. (a) Lasing spectra of 10 hexagonal cavities with the L from 9 to 18 μm. (b) Linear relationship between mode spacing $\Delta\lambda$ and $1/L$. (c) Edge perimeter-dependent pump threshold of $FAPbI_3$ polygonal microcavities with an error bar of ± 0.6 $\mu J/cm^2$.

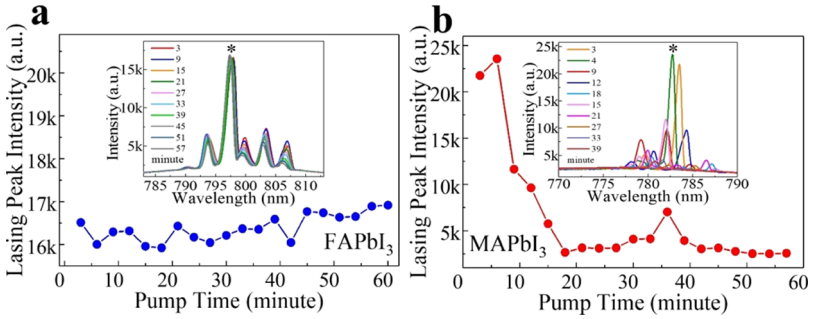

Figure 5. (a) Emission intensity of a single-square $FAPbI_3$ and (b) $MAPbI_3$ cavity under a 532 nm fs laser continuous illumination above P_{th} in an ambient atmosphere. Inset: the time-dependent lasing emission spectra in square microcavity with an edge length of 19 μm.

spectra of $MAPbI_3$ square cavity changed a lot (Figure 5b inset). These results indicate that $FAPbI_3$ polygon microcavity can achieve stable multimode lasing at room temperature.

As depicted in Figure S12, we tested angular dependence on the PL spectrum of $FAPbI_3$ polygon microcavity and the laser mode (marked with *) intensity as a function of polarizer angles (Figure S12 inset). Interestingly, we found the linear polarization in different polygonal microcavities like other research studies.[43−46] Moreover, we tested the polarization of polygonal microcavities at a thickness of 70 nm and proved that the polarization direction is sensitive to thickness, as seen in Figure S13.

In conclusion, triangular, square, pentagonal, and hexagonal $FAPbI_3$ polygonal microcavities are fabricated by using the fs laser-assisted writing method. The side faces of these polygonal microcavities constitute excellent built-in WGM microresonators for lasing. By using this straightforward, flexible, and repeatable scalable fabrication method, we find that with increasing the perimeter of $FAPbI_3$ polygonal microcavities at a limited range (about 48−108 μm), the lasing threshold will decrease. Furthermore, with microcavity polygonal order increasing, the lasing threshold and the fwhm are all decreasing. At last, the hexagonal $FAPbI_3$ microcavity exhibits the lowest pump threshold (~4.0 $\mu J/cm^2$) and the narrowest fwhm (~ 0.62 nm) among all polygonal microcavities, showing potential applications in narrow linewidth coherent light sources. These studies are important for understanding, improving, and engineering the microcavity devices to be applied in novel engineering.

■ ASSOCIATED CONTENT

Supporting Information

The Supporting Information is available free of charge at https://pubs.acs.org/doi/10.1021/acsami.0c21824.

AFM and cross-sectional SEM images of thermal-evaporated and spin-coated perovskite films; XRD patterns of evaporated $FAPbI_3$ perovskite films; Absorption spectrum and PL spectrum of evaporated $FAPbI_3$ perovskite films; Laser scanning confocal microscopy images and corresponding height profiles of individual $FAPbI_3$ microcavities; PL and lasing characterizations with a μ-PL system; Spot size of the laser beam; Emission spectra of $FAPbI_3$ triangle, square,

https://doi.org/10.1021/acsami.0c21824
ACS Appl. Mater. Interfaces 2021, 13, 16952−16958

pentagonal, and hexagonal microcavities at different intensities; and Polarization of the laser emission from various polygonal microcavities (PDF)

AUTHOR INFORMATION

Corresponding Authors

Qianqian Lin − *School of Physics and Technology, Wuhan University, Wuhan 430072, China;* orcid.org/0000-0002-6144-1761; Email: q.lin@whu.edu.cn

Qiang Cao − *The Institute of Technological Sciences, Wuhan University, Wuhan 430072, China;* orcid.org/0000-0002-5736-6893; Email: caoqiang@whu.edu.cn

Authors

Xiaoyu Tian − *The Institute of Technological Sciences, Wuhan University, Wuhan 430072, China*

Lin Wang − *Key Laboratory of Advanced Display and System Applications of Ministry of Education, Shanghai University, Shanghai 200072, China*

Wei Li − *School of Physics and Technology, Wuhan University, Wuhan 430072, China*

Complete contact information is available at: https://pubs.acs.org/10.1021/acsami.0c21824

Notes

The authors declare no competing financial interest.

ACKNOWLEDGMENTS

The authors thank Prof. L.X. for 3D morphology and roughness measurements of $FAPbI_3$ polygon microcavities. This work was financially supported by the Strategic Priority Research Program of the Chinese Academy of Sciences (grant no. XDA25040201), the National Natural Science Foundation of China (grant no. 51727901), the Natural Science Foundation of Hubei Province, China (grant nos. 2018CFA021 and 2019AAA020), the Fundamental Research Funds for the Central Universities (grant nos. 2042018kf0207 and 2042019kf0011), and the Wuhan Science and Technology Project of China (grant no. 2019010701011420).

REFERENCES

(1) Xing, G.; Mathews, N.; Lim, S. S.; Yantara, N.; Liu, X.; Sabba, D.; Grätzel, M.; Mhaisalkar, S.; Sum, T. C. Low-temperature solution-processed wavelength-tunable perovskites for lasing. *Nat. Mater.* **2014**, *13*, 476−480.

(2) Zhu, H.; Fu, Y.; Meng, F.; Wu, X.; Gong, Z.; Ding, Q.; Gustafsson, M. V.; Trinh, M. T.; Jin, S.; Zhu, X.-Y. Lead halide perovskite nanowire lasers with low lasing thresholds and high quality factors. *Nat. Mater.* **2015**, *14*, 636−642.

(3) Eaton, S. W.; Lai, M.; Gibson, N. A.; Wong, A. B.; Dou, L.; Ma, J.; Wang, L.-W.; Leone, S. R.; Yang, P. Lasing in robust cesium lead halide perovskite nanowires. *Proc. Natl. Acad. Sci. U.S.A.* **2016**, *113*, 1993−1998.

(4) Someya, T.; Werner, R.; Forchel, A.; Catalano, M.; Cingolani, R.; Arakawa, Y. Room temperature lasing at blue wavelengths in gallium nitride microcavities. *Science* **1999**, *285*, 1905−1906.

(5) Zhizhchenko, A. Y.; Tonkaev, P.; Gets, D.; Larin, A.; Zuev, D.; Starikov, S.; Pustovalov, E. V.; Zakharenko, A. M.; Kulinich, S. A.; Juodkazis, S.; Kuchmizhak, A. A.; Makarov, S. V. Light-emitting nanophotonic designs enabled by ultrafast laser processing of halide perovskites. *Small* **2020**, *16*, 2000410.

(6) Yamamoto, T.; Pashkin, Y. A.; Astafiev, O.; Nakamura, Y.; Tsai, J. S. Demonstration of conditional gate operation using superconducting charge qubits. *Nature* **2003**, *425*, 941−944.

(7) Strauf, S.; Hennessy, K.; Rakher, M. T.; Choi, Y. S.; Badolato, A.; Andreani, L. C.; Hu, E. L.; Petroff, P. M.; Bouwmeester, D. Self-tuned quantum dot gain in photonic crystal lasers. *Phys. Rev. Lett.* **2006**, *96*, 127404.

(8) Chen, R.; Bakti Utama, M. I.; Peng, Z.; Peng, B.; Xiong, Q.; Sun, H. Excitonic properties and near-infrared coherent random lasing in vertically aligned CdSe nanowires. *Adv. Mater.* **2011**, *23*, 1404−1408.

(9) Yang, J.; Liu, Z.; Pi, M.; Lin, H.; Zeng, F.; Bian, Y.; Shi, T.; Du, J.; Leng, Y.; Tang, X. High efficiency up-conversion random lasing from formamidinium lead bromide/amino-mediated silica spheres composites. *Adv. Opt. Mater.* **2020**, *8*, 2000290.

(10) Ma, R.-M.; Oulton, R. F.; Sorger, V. J.; Bartal, G.; Zhang, X. Room-temperature sub-diffraction-limited plasmon laser by total internal reflection. *Nat. Mater.* **2011**, *10*, 110−113.

(11) Huang, C.; Sun, W.; Fan, Y.; Wang, Y.; Gao, Y.; Zhang, N.; Wang, K.; Liu, S.; Wang, S.; Xiao, S.; Song, Q. Formation of lead halide perovskite based plasmonic nanolasers and nanolaser arrays by tailoring the substrate. *ACS Nano* **2018**, *12*, 3865−3874.

(12) Samuel, I. D. W.; Turnbull, G. A. Organic Semiconductor Lasers. *Chem. Rev.* **2007**, *107*, 1272−1295.

(13) Jia, Y.; Kerner, R. A.; Grede, A. J.; Brigeman, A. N.; Rand, B. P.; Giebink, N. C. Diode-pumped organo-lead halide perovskite lasing in a metal-clad distributed feedback resonator. *Nano Lett.* **2016**, *16*, 4624−4629.

(14) Humar, M.; Ravnik, M.; Pajk, S.; Muševič, I. Electrically tunable liquid crystal optical microresonators. *Nat. Photonics* **2009**, *3*, 595−600.

(15) McCall, S. L.; Levi, A. F. J.; Slusher, R. E.; Pearton, S. J.; Logan, R. A. Whispering-gallery mode microdisk lasers. *Appl. Phys. Lett.* **1992**, *60*, 289−291.

(16) Du, H.; Wang, K.; Zhao, L.; Xue, C.; Zhang, M.; Wen, W.; Xing, G.; Wu, J. Size-controlled patterning of single-crystalline perovskite arrays toward a tunable high-performance microlaser. *ACS Appl. Mater. Interfaces* **2020**, *12*, 2662−2670.

(17) Yang, Y.-D.; Tang, M.; Wang, F.-L.; Xiao, Z.-X.; Xiao, J.-L.; Huang, Y.-Z. Whispering-gallery mode hexagonal micro-/nanocavity lasers [Invited]. *Photon. Res.* **2019**, *7*, 594−607.

(18) Zhang, Q.; Ha, S. T.; Liu, X.; Sum, T. C.; Xiong, Q. Room-temperature near-infrared high-Q perovskite whispering-gallery planar nanolasers. *Nano Lett.* **2014**, *14*, 5995−6001.

(19) An, Y.; Shen, X.; Zhang, Y.; Liu, D.; Wu, Y.; Guo, P.; Zhou, W.; Hao, Y. *Color*-Tunable Photoluminescence and Whispering Gallery Mode Lasing of Alloyed $CsPbCl_3(_{1-x})Br_{3x}$ Microstructures. *Adv. Mater. Interfaces* **2020**, *7*, 1902126.

(20) Fang, H.-H.; Ding, R.; Lu, S.-Y.; Yang, Y.-D.; Chen, Q.-D.; Feng, J.; Huang, Y.-Z.; Sun, H.-B. Whispering-gallery mode lasing from patterned molecular single-crystalline microcavity array. *Laser Photon. Rev.* **2013**, *7*, 281−288.

(21) Mi, Y.; Jin, B.; Zhao, L.; Chen, J.; Zhang, S.; Shi, J.; Zhong, Y.; Du, W.; Zhang, J.; Zhang, Q.; Zhai, T.; Liu, X. High-quality hexagonal nonlayered CdS nanoplatelets for low-threshold whispering-gallery-mode lasing. *Small* **2019**, *15*, 1901364.

(22) Mi, Y.; Wu, Y.; Shi, J.; Luo, S.-N. Robust single-mode lasers based on hexagonal CdS microflakes. *J. Mater. Chem. C* **2020**, *8*, 11201−11208.

(23) Yang, Y.; Huang, Y. Symmetry analysis and numerical simulation of mode characteristics for equilateral-polygonal optical microresonators. *Phys. Rev. A* **2007**, *76*, 023822.

(24) Li, G.; Che, T.; Ji, X.; Liu, S.; Hao, Y.; Cui, Y.; Liu, S. Record-low-threshold lasers based on atomically smooth triangular nanoplatelet perovskite. *Adv. Funct. Mater.* **2019**, *29*, 1805553.

(25) Zhang, Q.; Liu, X.; Xing, J.; Sum, T.; Xiong, Q. High-quality whispering-gallery-mode lasing from cesium lead halide perovskite nanoplatelets. *Adv. Funct. Mater.* **2016**, *26*, 6238−6245.

(26) Liu, M.; Johnston, M. B.; Snaith, H. J. Efficient planar heterojunction perovskite solar cells by vapour deposition. *Nature* **2013**, *501*, 395−398.

(27) Ball, J. M.; Buizza, L.; Sansom, H. C.; Farrar, M. D.; Klug, M. T.; Borchert, J.; Patel, J.; Herz, L. M.; Johnston, M. B.; Snaith, H. J.

Dual-Source Coevaporation of Low-Bandgap $FA_{1-x}Cs_xSn_{1-y}Pb_yI_3$ Perovskites for Photovoltaics. *ACS Energy Lett.* **2019**, *4*, 2748−2756.
(28) Li, J.; Wang, H.; Chin, X. Y.; Dewi, H. A.; Vergeer, K.; Goh, T. W.; Lim, J. W. M.; Lew, J. H.; Loh, K. P.; Soci, C.; Sum, T. C.; Bolink, H. J.; Mathews, N.; Mhaisalkar, S.; Bruno, A. Highly efficient thermally co-evaporated perovskite solar cells and mini-modules. *Joule* **2020**, *4*, 1035−1053.
(29) Li, J.; Du, P.; Li, S.; Liu, J.; Zhu, M.; Tan, Z.; Hu, M.; Luo, J.; Guo, D.; Ma, L.; Nie, Z.; Ma, Y.; Gao, L.; Niu, G.; Tang, J. High-throughput combinatorial optimizations of perovskite light-emitting diodes based on all-vacuum deposition. *Adv. Funct. Mater.* **2019**, *29*, 1903607.
(30) Min, H.; Kim, M.; Lee, S.-U.; Kim, H.; Kim, G.; Choi, K.; Lee, J. H.; Seok, S. I. Efficient, stable solar cells by using inherent bandgap of α-phase formamidinium lead iodide. *Science* **2019**, *366*, 749−753.
(31) Fu, M.; Tamarat, P.; Trebbia, J. B.; Bodnarchuk, M. I.; Kovalenko, M. V.; Even, J.; Lounis, B. Unraveling exciton-phonon coupling in individual FAPbI3 nanocrystals emitting near-infrared single photons. *Nat. Commun.* **2018**, *9*, 3318.
(32) Fu, Y.; Zhu, H.; Schrader, A. W.; Liang, D.; Ding, Q.; Joshi, P.; Hwang, L.; Zhu, X.-Y.; Jin, S. Nanowire lasers of formamidinium lead halide perovskites and their stabilized alloys with improved stability. *Nano Lett.* **2016**, *16*, 1000−1008.
(33) Li, X.; Wang, K.; Chen, M.; Wang, S.; Fan, Y.; Liang, T.; Song, Q.; Xing, G.; Tang, Z. Stable whispering gallery mode lasing from solution-processed formamidinium lead bromide perovskite microdisks. *Adv. Opt. Mater.* **2020**, *8*, 2000030.
(34) Polson, R. C.; Levina, G.; Vardeny, Z. V. Spectral analysis of polymer microring lasers. *Appl. Phys. Lett.* **2000**, *76*, 3858−3860.
(35) Gargas, D. J.; Moore, M. C.; Chang, S.-W.; Zhang, Z.; Chuang, S.-L.; Yang, P. Whispering gallery mode lasing from zinc oxide hexagonal nanodisks. *ACS Nano* **2010**, *4*, 3270−3276.
(36) Di, D.; Musselman, K. P.; Li, G.; Sadhanala, A.; Ievskaya, Y.; Song, Q.; Tan, Z.-K.; Lai, M. L.; MacManus-Driscoll, J. L.; Greenham, N. C.; Friend, R. H. Size-dependent photon emission from organometal halide perovskite nanocrystals embedded in an organic matrix. *J. Phys. Chem. Lett.* **2015**, *6*, 446−450.
(37) Tian, X.; Xu, Y.; Zhao, H.; Qin, X.; Nie, Y.; Li, W.; Liu, S.; Lin, Q.; Cao, Q. Femtosecond laser direct writing of perovskite patterns with whispering gallery mode lasing. *J. Mater. Chem. C* **2020**, *8*, 7314−7321.
(38) Bhowmik, A. K. Polygonal optical cavities. *Appl. Opt.* **2000**, *39*, 3071−3075.
(39) Wiersig, J. Hexagonal dielectric resonators and microcrystal lasers. *Phys. Rev. A* **2003**, *67*, 023807.
(40) Czekalla, C.; Nobis, T.; Rahm, A.; Cao, B.; Zúñiga-Pérez, J.; Sturm, C.; Schmidt-Grund, R.; Lorenz, M.; Grundmann, M. Whispering gallery modes in zinc oxide micro- and nanowires. *Phys. Status Solidi B* **2010**, *247*, 1282−1293.
(41) Yamamoto, Y.; Machida, S.; Björk, G. Microcavity semiconductor laser with enhanced spontaneous emission. *Phys. Rev. A* **1991**, *44*, 657−668.
(42) Triviño, N. V.; Butté, R.; Carlin, J.-F.; Grandjean, N. Continuous wave blue lasing in III-nitride nanobeam cavity on silicon. *Nano Lett.* **2015**, *15*, 1259−1263.
(43) Zhu, H.; Fu, Y.; Meng, F.; Wu, X.; Gong, Z.; Ding, Q.; Gustafsson, M. V.; Trinh, M. T.; Jin, S.; Zhu, X.-Y. Lead halide perovskite nanowire lasers with low lasing thresholds and high quality factors. *Nat. Mater.* **2015**, *14*, 636−642.
(44) Chen, S.; Nurmikko, A. Stable green perovskite vertical-cavity surface-emitting lasers on rigid and flexible substrates. *ACS Photonics* **2017**, *4*, 2486−2494.
(45) Huang, C.; Sun, W.; Fan, Y.; Wang, Y.; Gao, Y.; Zhang, N.; Wang, K.; Liu, S.; Wang, S.; Xiao, S.; Song, Q. Formation of lead halide perovskite based plasmonic nanolasers and nanolaser arrays by tailoring the substrate. *ACS Nano* **2018**, *12*, 3865−3874.
(46) Duan, Z.; Wang, Y.; Li, G.; Wang, S.; Yi, N.; Liu, S.; Xiao, S.; Song, Q. Chip-Scale fabrication of uniform lead halide perovskites microlaser array and photodetector array. *Laser Photon. Rev.* **2018**, *12*, 1700234.

https://doi.org/10.1021/acsami.0c21824
ACS Appl. Mater. Interfaces 2021, 13, 16952−16958